Injection-locking of terahertz quantum cascade lasers up to 35GHz using RF amplitude modulation

Pierre Gellie[1], Stefano Barbieri[1*], Jean-François Lampin[2], Pascal Filloux[1], Christophe Manquest[1], Carlo Sirtori[1], Isabelle Sagnes[3], Suraj P. Khanna[4], Edmund H. Linfield[4], A. Giles Davies[4], Harvey Beere[5], David Ritchie[5]

[1]Laboratoire Matériaux et Phénomènes Quantiques, Université Paris 7and CNRS UMR 7162, 10 rue A. Domont et L. Duquet, 75205 Paris, France
[2]Institut d'Electronique de Microélectronique et de Nanotechnologie (IEMN), CNRS UMR 8520 Université de Lille 1, Avenue Poincaré B.P. 60069, 59652 Villeneuve d'Ascq, France
[3]Laboratoire LPN, Route de Nozay, 91460 Marcoussis, France
[4]Cavendish Laboratory, J. J. Thomson Avenue, Cambridge CB3 0HE, United Kingdom
[5]School of Electronic and Electrical Engineering, University of Leeds,Leeds LS2 9JT, United Kingdom
[*stefano.barbieri@univ-paris-diderot.fr](mailto:stefano.barbieri@univ-paris-diderot.fr)

Abstract: We demonstrate that the cavity resonance frequency –the round-trip frequency – of Terahertz quantum cascade lasers can be injection-locked by direct modulation of the bias current using an RF source. Metal-metal and single-plasmon waveguide devices with roundtrip frequencies up to 35GHz have been studied, and show locking ranges above 200MHz. Inside this locking range the laser round-trip frequency is phase-locked, with a phase noise determined by the RF-synthesizer. We find a square-root dependence of the locking range with RF-power in agreement with classical injection-locking theory. These results are discussed in the context of mode-locking operation.

©2010 Optical Society of America

OCIS codes: (000.2700) General science.

References and links

1. E. A. Avrutin, J. H. Marsh, and E. L. Portnoi, "Monolithic and multi-GigaHertz mode-locked semiconductor lasers: constructions, experiments, models and applications," IEE Proc., Optoelectron. **147**(4), 251–278 (2000).
2. J. E. Bowers, P. A. Morton, A. Mar, and S. W. Corzine, "Actively mode-locked semiconductor lasers," IEEE J. Quantum Electron. **25**(6), 1426–1439 (1989).
3. L. A. Jiang, M. E. Grein, E. P. Ippen, C. McNeilage, J. Searls, and H. Yokoyama, "Quantum-limited noise performance of a mode-locked laser diode," Opt. Lett. **27**(1), 49–51 (2002).
4. D. Y. Kim, D.-S. Seo, and H.-F. Liu, "Observation of very efficeint hybrid mode-locking in InGaAs/InGaAsInP multiple quantum well distributed Bragg reflector laser diode," Appl. Phys. Lett. **67**(21), 3075–3077 (1995).
5. S. Arahira, and Y. Ogawa, "Synchronous mode-locking in passively mode-locked semiconductor laser diodes using optical short pulses repeated at subharmonics of the cavity round-trip frequency," IEEE Photon. Technol. Lett. **8**(2), 191–193 (1996).
6. T. Hoshida, H-F. Liu, M. Tsuchiya, Y. Ogawa, T. Kamiya, "Subharmonic Hybrid Mode-Locking of a Monolithic Semiconductor Laser," IEEE J. Selected Topics Quantum. Electron.
7. R. Paiella, "Intersubband transitions in quantum structures" Mc-Graw Hill Nanoscience and Technology, New York (2006)
8. R. Paiella, R. Martini, F. Capasso, C. Gmachl, H. Y. Hwang, D. L. Sivco, J. N. Ballargeon, A. Y. Cho, E. A. Whyttaker, and H. C. Liu, "High-frequency modulation without the relaxation oscillation resonance in quantum cascade lasers," Appl. Phys. Lett. **79**(16), 2526–2528 (2001).
9. R. Paiella, F. Capasso, C. Gmachl, H. Y. Hwang, D. L. Sivco, A. L. Hutchinson, A. Y. Cho, and H. C. Liu, "Monolithic active mode-locking of quantum cascade lasers," Appl. Phys. Lett. **77**(2), 169–171 (2000).
10. C. Y. Wang, L. Kuznetsova, V. M. Gkortsas, L. Diehl, F. X. Kärtner, M. A. Belkin, A. Belyanin, X. Li, D. Ham, H. Schneider, P. Grant, C. Y. Song, S. Haffouz, Z. R. Wasilewski, H. C. Liu, and F. Capasso, "Mode-locked pulses from mid-infrared quantum cascade lasers," Opt. Express **17**(15), 12929–12943 (2009).
11. S. Kumar, Q. Hu, and J. L. Reno, "186 K operation of terahertz quantum-cascade lasers based on a diagonal design," Appl. Phys. Lett. **94**(13), 131105 (2009).
12. G. Scalari, C. Walther, M. Fischer, R. Terazzi, H. Beere, D. Ritchie, and J. Faist, "THz and sub-THz quantum cascade lasers," Laser Photon Rev. **3**(1-2), 45–66 (2009).

13. B. S. Williams, "Terahertz quantum cascade lasers," Nat. Photonics **1**(9), 517–525 (2007).
14. W. Maineult, L. Ding, P. Gellie, P. Filloux, C. Sirtori, S. Barbieri, J. F. Lampin, T. Akalin, I. Sagnes, H. E. Beere, and D. A. Ritchie, "Microwave modulation of THz quantum cascade lasers: a transmission−line approach," Appl. Phys. Lett. **96**(2), 021108–021110 (2010).
15. S. Barbieri, W. Maineult, S. S. Dhillon, C. Sirtori, J. Alton, N. Breuil, H. E. Beere, and D. A. Ritchie, "13 GHz direct modulation of terahertz quantum cascade lasers," Appl. Phys. Lett. **91**(14), 143510 (2007).
16. M. Hajenius, P. Khosropanah, J. N. Hovenier, J. R. Gao, T. M. Klapwijk, S. Barbieri, S. Dhillon, P. Filloux, C. Sirtori, D. A. Ritchie, and H. E. Beere, "Surface plasmon quantum cascade lasers as terahertz local oscillators," Opt. Lett. **33**(4), 312–314 (2008).
17. T. Yilmaz, C. M. Depriest, P. J. Delfyett, Jr., A. Braun, and J. Abeles, "Measurement of residual phase noise and longitudinal-mode linewidth in a hybridly mode-locked external linear cavity semiconductor laser," Opt. Lett. **27**(10), 872–874 (2002).
18. C. Worrall, J. Alton, M. Houghton, S. Barbieri, H. E. Beere, D. Ritchie, and C. Sirtori, "Continuous wave operation of a superlattice quantum cascade laser emitting at 2 THz," Opt. Express **14**(1), 171–181 (2006).
19. The origin of these sidebands is not clear. However they are not relevant for this work.
20. S. Barbieri, J. Alton, C. Baker, T. Lo, H. Beere, and D. Ritchie, "Imaging with THz quantum cascade lasers using a Schottky diode mixer," Opt. Express **13**(17), 6497–6503 (2005).
21. S. Barbieri, W. Maineult, L. Ding, P. Gellie, P. Filloux, C. Sirtori, T. Akalin, J. F. Lampin, I. Sagnes, H. E. Beere, and D. A. Ritchie, "Microwave technology applied to THz quantum cascade lasers," Proc. SPIE **7608**, 76080X (2010).
22. A. E. Siegman, "Lasers", University Science Books, Mill Valley, (1986).
23. Z. Ahmed, L. Zhai, A. J. Lowery, N. Onodera, and R. S. Tucker, "Locking bandwidth of actively mode-locked semiconductor lasers," IEEE J. Quantum Electron. **29**(6), 1714–1721 (1993).
24. As mentioned above in the text, the oscillation in the intensity of f_{RF} is produced by the non-ideal directivity of the coupler (Fig. 2(a)).
25. M. DiDomenico, Jr., "Small-signal analysis of internal (coupling-type) modulation of lasers," J. Appl. Phys. **35**(10), 2870–2876 (1964).
26. O. P. McDuff, and S. E. Harris, "Nonlinear theory of internally loss-modulated lasers," IEEE J. Quantum Electron. **3**(3), 101–111 (1967).
27. R. Adler, "A study of locking phenomena in oscillators," Proc. IEEE **61**(10), 1380–1385 (1973).
28. B. Razavi, "A study of injection-locking and pulling in oscillators," IEEE J. Sol. State Circuits. **39**(9), 1415–1424 (2004).
29. S. Kohen, B. S. Williams, and Q. Hu, "Electromagnetic modeling of terahertz quantum cascade laser waveguides and resonators," Appl. Phys. Lett. **97**, 053106–053108 (2005).
30. S. Barbieri, J. Alton, J. Fowler, H. E. Beere, E. H. Linfield, and D. A. Ritchie, "2.9 THz quantum cascade lasers operating up to 70 K in continuous wave," Appl. Phys. Lett. **85**(10), 1674 (2004).
31. M. Hajenius, P. Khosropanah, J. N. Hovenier, J. R. Gao, T. M. Klapwijk, S. Barbieri, S. Dhillon, P. Filloux, C. Sirtori, D. A. Ritchie, and H. E. Beere, "Surface plasmon quantum cascade lasers as terahertz local oscillators," Opt. Lett. **33**(4), 312–314 (2008).
32. S. Barbieri, J. Alton, H. E. Beere, E. H. Linfield, D. A. Ritchie, S. Withington, G. Scalari, L. Ajili, and J. Faist, "Heterodyne mixing of two far-infrared quantum cascade lasers by use of a point-contact Schottky diode," Opt. Lett. **29**(14), 1632–1634 (2004).
33. A. Barkan, F. K. Tittel, D. M. Mittleman, R. Dengler, P. H. Siegel, G. Scalari, L. Ajili, J. Faist, H. E. Beere, E. H. Linfield, A. G. Davies, and D. A. Ritchie, "Linewidth and tuning characteristics of terahertz quantum cascade lasers," Opt. Lett. **29**(6), 575–577 (2004).
34. S. Barbieri, P. Gellie, G. Santarelli, L. Ding, W. Maineult, C. Sirtori, R. Colombelli, H. E. Beere, and D. A. Ritchie, "Phase locking of a 2.7THz quantum cascade laser to a mode-locked Er-fiber laser," Nature Photonics **4**, 636 - 640 (2010).
35. E. E. Orlova, J. N. Hovenier, T. O. Klaassen, I. Ksalynas, A. J. L. Adam, J. R. Gao, T. M. Klapwijk, B. S. Williams, S. Kumar, Q. Hu, and J. L. Reno, Phys. Rev. Lett. **96**, "Antenna model for wire-lasers," 173904 −173906 (2006).
36. W. Maineult, P. Gellie, A. Andronico, P. Filloux, G. Leo, C. Sirtori, S. Barbieri, E. Peytavit, T. Akalin, J.-F. Lampin, J. Alton, H. Beere, and D. R. Ritchie, "Double metal quantum cascade lasers with micro-TEM horn antenna," Appl. Phys. Lett. **93**(18), 183508 (2008).
37. Compared to Section 2, for the measurements presented in this Section we used a different SA with a higher resolution (1Hz compared to 10Hz).
38. We tried using longer devices. Unfortunately the cooling power needed to cool the QCLs was beyond the capability of our cryostat.
39. R. Paiella, F. Capasso, C. Gmachl, D. L. Sivco, J. N. Baillargeon, A. L. Hutchinson, A. Y. Cho, and H. C. Liu, "Self-mode-locking of quantum cascade lasers with giant ultrafast optical nonlinearities," Science **290**(5497), 1739–1742 (2000).
40. C. Y. Wang, L. Diehl, A. Gordon, C. Jirauschek, F. X. Kärtner, A. Belyanin, D. Bour, S. Corzine, G. Höfler, M. Troccoli, J. Faist, and F. Capasso, "Coherent instabilities in a semiconductor laser with fast gain recovery," Phys. Rev. A **75**(3), 031802 (2007).
41. H. Choi, L. Diehl, Z. K. Wu, M. Giovannini, J. Faist, F. Capasso, and T. B. Norris, "Gain recovery dynamics and photon-driven transport in quantum cascade lasers," Phys. Rev. Lett. **100**(16), 167401 (2008).

42. M. Amanti, G. Scalari, R. Terazzi, M. Fischer, M. Beck, J. Faist, A. Rudra, P. Gallo, and E. Kapon, "Bound-to-continuum terahertz quantum cascade laser with a single-quantum-well phonon extraction/injection stage," N. J. Phys. **11**(12), 1–19 (2009).
43. C. Walther, G. Scalari, J. Faist, H. Beere, and D. Ritchie, "Low frequency terahertz quantum cascade laser operating from 1.6 to 1.8 THz," Appl. Phys. Lett. **89**(23), 231121 (2006).
44. C. Walther, M. Fisher, G. Scalari, R. Terazzi, N. Hoyler, and J. Faist, "Quantum cascade laser operating from 1.2 to 1.6 THz," Appl. Phys. Lett. **91**(13), 131122 (2007).
45. S. Ramo, J. R. Whinnery, and T. V. Duzer, "Field and waves in communication electronics," 2nd ed. (Wiley, 1984).

1. Introduction

Stabilization of the round-trip frequency of mode-locked laser diodes (LDs) by electrical modulation, also called *RF injection-locking*, has been studied extensively during the 1990s for applications in microwave-over-fiber transmission, such as optical analog-to-digital conversion and optical clock recovery, where the pulse-to-pulse timing jitter is critically important [1,2]. It is well known that in mode-locked lasers the frequency and phase-stability of the cavity roundtrip frequency (f_{rt}), is directly related to the stability of the timing-jitter of the emitted pulse train [2,3]. Effective stabilization was generally achieved using hybrid mode-locking schemes, where a passively mode-locked LD is stabilized by
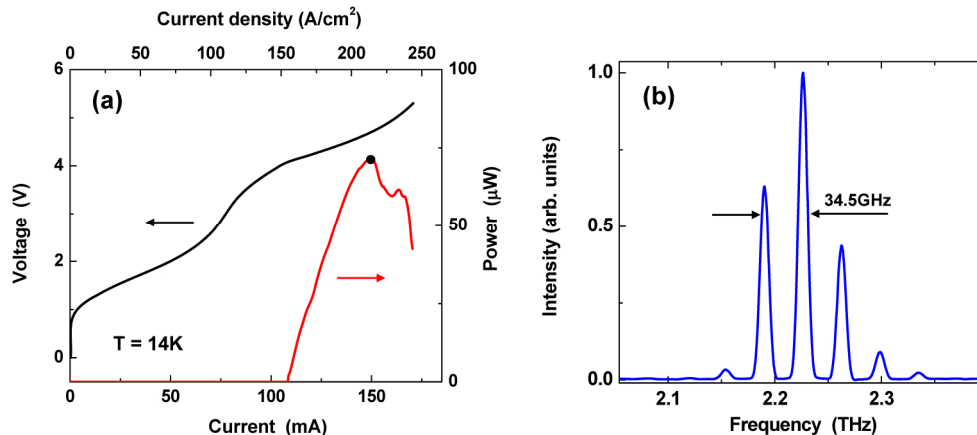
Fig. 1. Metal-metal waveguide QCL. The device is 1.0mm-long and 70μm wide. (a) Continuous-wave (CW) Voltage/Current and Optical-power/Current characteristics at a heat-sink temperature of 10K. (b) Representative THz emission spectrum measured at a current of 150mA (black dot in panel(a)). The FP modes are separated by approximately 34.5GHz.

applying an RF modulation to a short saturable absorber section rather than the laser gain section itself. In this way the intrinsic modulation cutoff caused by the relaxation-oscillations in the gain medium can be overcome, and highly stable pulse trains at repetition rates of several tens of GHz achieved with RF-powers below 0dBm [1,4–6]. In the best cases, the linewidth of f_{rt}, typically in the 0.1 – 1MHz range for passive mode-locking operation, can then have a value comparable to that of the driving RF source.

Quantum Cascade Lasers (QCLs) are unipolar semiconductor lasers based on electronic intersubband transitions in the conduction band of multi-layered heterostructures [7]. As such their physical properties are drastically different from those of classical interband LDs. For instance they are characterized by non-radiative recombination times on the ps timescale, which have a dramatic impact on their dynamics. In particular, in contrast to interband LDs, over-damped relaxation oscillations leading to a flat intrinsic modulation frequency response function up to several tens of GHz are expected [8]. Neglecting parasitic effects due to the device packaging, these physical properties in principle allow efficient direct amplitude modulation (AM) of the gain medium, which could be used for RF injection-locking up to several tens of GHz.

The first demonstration of AM of a QCL was reported with devices emitting at 8µm [9]. In this work an enhancement in the number of the longitudinal Fabry-Pérot (FP) lasing modes was observed when the RF modulation frequency f_{RF} was brought close to f_{rt} ~13GHz. The spectral width of f_{rt} was always large, however, with values of several tens of MHz in the best case. Such values are not compatible with stable mode-locked operation. Subsequently, a ~3kHz wide peak was measured at f_{rt}~17.8GHz in the photocurrent spectrum of an actively mode-locked 2.6mm-long QCL emitting at 6.3µm [10].
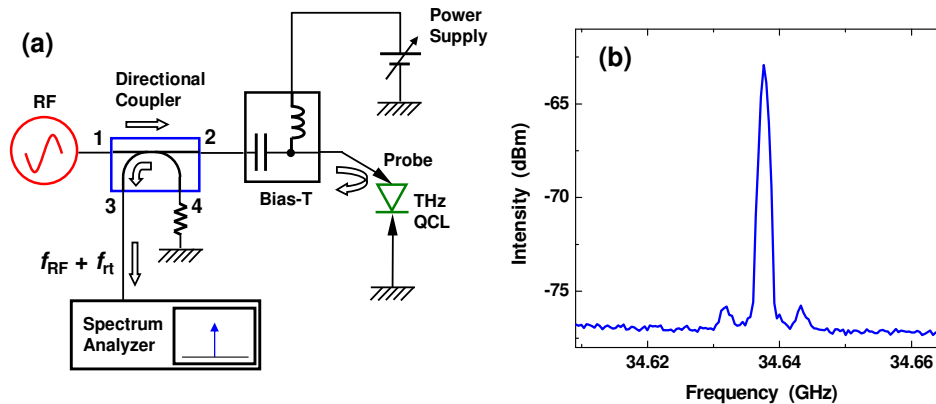
Fig. 2. **(a)** Metal-metal QCL. Schematic of the measurement setup for the RF injection-locking. An RF-synthesizer (Agilent E8257D) is connected to the input port (port 1) of a 40GHz directional coupler. Port 2 of the coupler is connected to the *ac* input of a 60GHz bias-T. The *dc* input of the bias-T is connected to a power supply that drives the QCL at constant current. The RF and dc-bias signals are brought to the QCL via a 60GHz, 50Ω coplanar probe positioned at one end of the QCL ridge. The signal from the RF generator is partially reflected at the QCL/coplanar probe boundary and, together with the beat-note at f_{rt}, is monitored on a spectrum analyzer (SA) connected to port 3 of the coupler. The total attenuation from the RF generator to the QCL (including the 1dB transmission loss at the QCL/probe boundary) is of 14dB. **(b)** RF-spectrum collected with the RF-source switched OFF, and using a RBW of 100kHz, a sweep time of 1s on a 300MHz span, and with the RMS detection mode switched ON. The central peak at 34.637GHz has a resolution-limited 3dB-linewidth of ~1MHz.

Recently, we have shown that terahertz (THz) frequency QCLs [11–13] based on metal-metal waveguides are more suitable for AM in comparison with mid-IR devices [14,15]. In fact the metal-metal waveguide is essentially a downscaled version of a standard microwave microstrip-waveguide, and provides a nearly 100% overlap factor, across the GHz to THz frequency range, of the fundamental TEM mode with the active region. These excellent confinement properties are combined with relatively small amplitude attenuations at GHz frequencies (~2.5dB/mm at 40GHz, see Ref [14].), owing to the fact that in THz QCLs the doping level of the active region is very low. These properties have recently led to the direct AM up to 24GHz of a metal-metal waveguide 2.3THz QCL [14].

In this work we have further exploited the RF-modulation capabilities of metal-metal waveguide THz QCLs to demonstrate that their roundtrip frequency can be effectively injection-locked to a microwave-synthesizer. By direct AM-modulation of a 2.3THz QCL processed into a 1mm-long ridge, locking could be achieved at 35GHz with input RF-powers <-15dBm, and locking ranges in excess of 200MHz were obtained at −10dBm. We find that inside the locking range f_{rt} is phase-locked to the RF synthesizer. These results are presented in Section 2. Section 3 is dedicated instead to the RF injection-locking of a single-plasmon waveguide QCL emitting at 2.4THz. Although less suitable for GHz modulation, THz QCLs employing single-plasmon waveguides have vastly superior beam properties, compared with metal-metal waveguide ridges. Directional and relatively symmetrical beams are normally achieved, with angular divergences of ~20-30°, that allow nearly diffraction-limited focusing of the emitted radiation [16]. Contrary to the metal-metal device, where for the detection of f_{rt}

we used a non-linearity intrinsic to the device electrical characteristic (see the next Section for details), we have taken advantage of these good beam properties to couple the single-plasmon QCL radiation to a Schottky mixer. This has allowed us to probe not only the locking characteristics but also the optical modulation response function of the device.
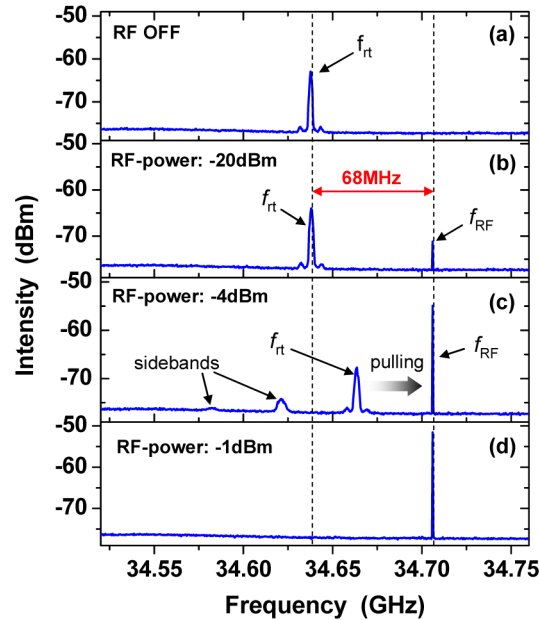
Fig. 3. Metal-metal QCL. RF injection-locking of f_{rt}. The spectra were collected with the same settings of Fig. 2(b) (a) The RF-source is switched OFF and $f_{rt} = 34.637$GHz. (b) RF-power of -20dBm, (i.e about -34dBm inside the device) and $f_{RF} = 34.706$GHz, 68MHz on the right of f_{rt}. (c) RF-power of -4dBm. f_{rt} is pulled by ~27MHz towards f_{RF}. Two sidebands appear on the left side of f_{rt} All the lines are separated by $f_b = 42$MHz. (d) RF-power of -1dBm. f_{rt} is injection locked by the RF-source.

Apart from being potentially relevant for applications in THz wireless communication and THz metrology, the possibility of phase-locking f_{rt} to a stable-microwave synthesizer through direct AM that we demonstrate in this work, is a significant step towards the active mode-locking of THz QCLs. Indeed, the injection of f_{rt} implies automatically that the longitudinal FP modes are mutually phase-locked. As a consequence the QCL is operating in a regime of active-mode-locking, with a timing jitter of the emitted pulse train determined by the phase-noise of the RF-source [2,3,17].

2. RF Injection-locking of metal-metal waveguide THz QCLs

To study injection locking in a THz QCL with a metal-metal waveguide, we used a device with a multi-mode emission spectrum centered at ~2.2 THz. The active region is composed of 110 repeat periods of the structure described in Ref [18], and is inserted between 70nm and 600nm-thick top and bottom contact layers, n-doped to 5×10^{18} cm^{-3} and 1×10^{18} cm^{-3}, respectively. Devices were processed into metal-metal waveguides using ICP etching, resulting into 70μm-wide and 16.2μm-thick ridges sandwiched between an Au bottom ground plane and Ti/Au top layer. Ridges were cleaved into 1.0mm-long FP cavities, and indium-bonded onto copper-holders for thermal heat-sinking. For the injection-locking experiment the copper holder was screwed onto the cold-plate of a cryogenic probe station
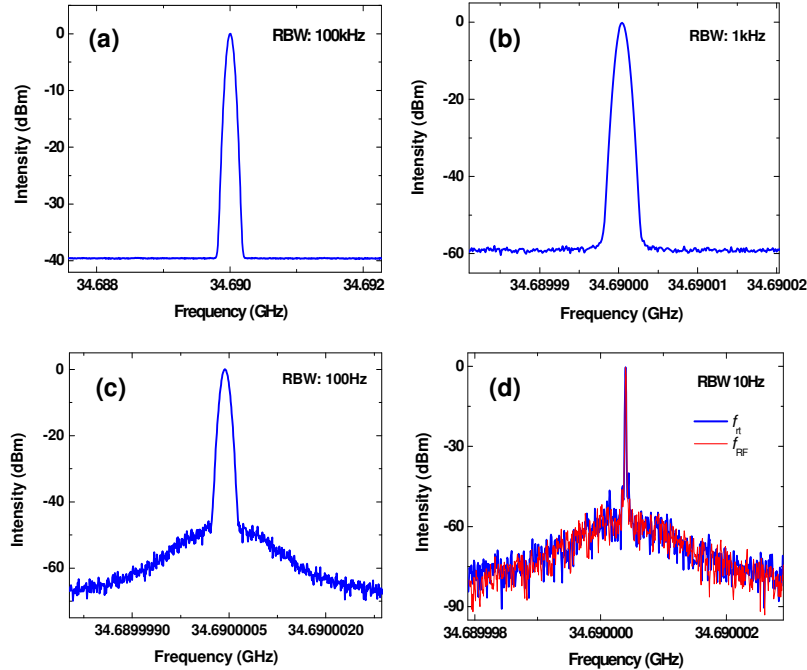
Fig. 4. Metal-metal QCL. Spectra at −2dBm RF-power, of the injection-locked roundtrip frequency measured with increasing RBW of the SA from 100kHz (a) to 10Hz (d), the spectral resolution limit of the SA. Spectra where collected in RMS detection mode, with a 50s sweep time. The peak intensity was normalized at 0dBm. In panel (d) the spectrum of the locked f_{rt} (blue) is shown together with the spectrum of f_{RF} (red).

with no optical (THz) access, and measurements were performed at 4K with the help of a coplanar probe. For the measurement of the THz spectra the device was subsequently wire-bonded and mounted on the cold head of a continuous flow He-cryostat with optical access. Spectra were measured with a Fourier transform spectrometer with a resolution of 0.25cm^{-1} (7.5GHz). The electrical and optical characteristics of the device operated in continuous-wave at 10K are shown in Fig. 1 on a linear scale. The threshold current is of 105mA and the maximum power is emitted at approximately 150mA. One representative spectrum collected at a current of 150mA is shown on panel (b) in linear scale. Six longitudinal FP modes are clearly evident, separated by the cavity f_{rt} of approximately 34.5GHz.

Figure 2(a) shows a schematic of the measurement setup for the RF injection-locking. An RF-synthesizer (Agilent E8257D) is connected through a directional coupler to a bias-tee that allows AM of the QCL, with the latter driven at constant current using a standard power supply. The RF + dc-bias signal is brought to the QCL via a 60GHz, 50Ω coplanar probe positioned at one end of the ridge, with the other end left open-ended. The device RF-impedance had been previously fully characterized in the 0-55GHz range using a vectorial network analyzer (see Ref [14].). Close to ~34.5GHz we obtain a power transmission coefficient of 0.8 (i.e. ~1dB transmission loss). One port of the coupler (labeled '3′ in Fig. 2) is connected to a 67 GHz Rohde & Schwarz Spectrum Analyzer (SA). As indicated by the arrows in Fig. 2, this allows a continuous monitoring of the RF-synthesizer signal at f_{RF} as a fraction of the power (0.2) is reflected by the impedance mismatch at the QCL input facet. We note that in all the RF spectra shown in this Section the intensities of the peaks are affected by a non-ideal directivity of the coupler. This produces an interference effect between the wave emitted by the RF-generator that is parasitically transmitted from port n.1 to port n. 3, and the reflected wave from the QCL (see also Fig. 6). For this reason, although the power transmitted to the QCL is virtually independent from the RF frequency, it is not possible to deduce

absolute intensities from the spectra recorded by the SA. Using a power meter we measured power attenuations of 13dB from the RF-source to the QCL and of 23dB from the QCL to the SA.
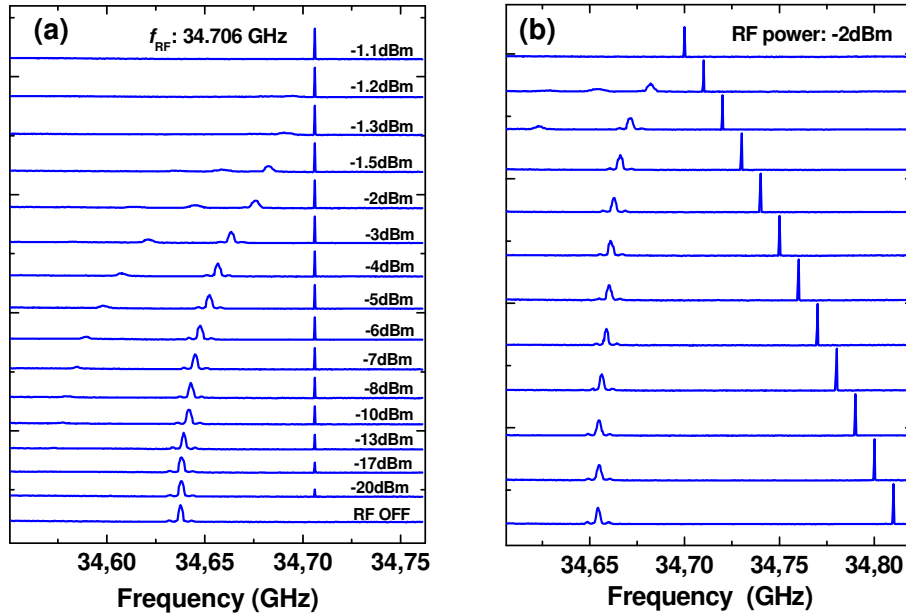
Fig. 5. Metal-metal QCL. Pulling and locking of f_{rt}. (a) f_{RF} is fixed at 34.706GHz and the RF-power is increased from −20dBm to −1.1dBm. (b) the RF-power is fixed at −2dBm and f_{RF} goes from 34.82GHz (bottom) to 34.70GHz (top). All the spectra were collected with the same settings of Fig. 2(b).

For all the measurements the QCL was driven at 150mA, at a heat-sink temperature of 14K. Figure 2(b) shows an RF-spectrum collected with the RF-source switched off, and using a resolution bandwidth (RBW) of 100 kHz, a sweep time of 1s, and with the RMS mode of the SA switched ON. A high intensity peak at 34.637GHz is clearly visible in the center, with a resolution-limited 3dB linewidth of ~1MHz. Nearly 15dBm below, two additional sidebands appear at approximately ± 6MHz [19]. By comparison with the THz spectrum of Fig. 1(b) we observe that the frequency of the peak in Fig. 2(b) coincides with f_{rt}, i.e. the separation between the longitudinal FP modes. In agreement with previous data (see Ref [20,21].), we interpret the appearance of the peak of Fig. 2(b) to be the result of a rectification of the THz intracavity field by the intrinsic non-linearity of the QCL voltage-current characteristic, that gives rise to an RF signal through the beating of neighboring FP modes. With interband DLs, f_{rt} is generally detected by focusing the laser radiation on a fast photodiode connected to a SP [5,6]. In this case the quadratic detection associated with interband absorption provides the rectification mechanism. In contrast, here, the detection process is directly performed by the device itself, producing an RF beat-note at the QCL voltage probes without the need of an external detector. The fairly simple setup of Fig. 2(b) therefore allows the RF-source signal and f_{rt} to be monitored simultaneously.

Fig. 6. Metal-metal QCL. (Media 1) Video sample of the SA screen. The RF-power is of −2dBm. f_{RF} is swept at constant speed from the low frequency side (from left to right on the screen). The frequency scale is of 100MHz/div. The intensity scale is of 10dB/div. The oscillations of the intensity of the RF signal are the consequence of an interference effect due to the non-ideal directivity of the coupler shown in Fig. 2 (see text).

Figure 3 illustrates the RF injection-locking of f_{rt} with four representative spectra collected with the same parameters used for Fig. 2(b). Figure 3(a) is identical to the spectrum presented in Fig. 2(b), with the RF-source switched OFF and f_{rt} = 34.637GHz. In Fig. 3(b) the RF-source is switched on with an output power of −20dBm, (i.e. about −34dBm inside the device). A spectral line corresponding to f_{RF} = 34.706GHz appears 68 MHz to the right of f_{rt}. Increasing the RF power to −4 dBm pulls f_{rt} by ~27 MHz towards f_{RF}, from the free-running value of 34.637 GHz → 34.664 GHz (Fig. 3(c)). In addition, two sidebands are generated on the left side of the spectrum. All the lines are separated by f_b = 42MHz, given by the difference between f_{RF} and the pulled f_{rt}. At −1 dBm, f_{rt} is injection locked by the RF-source (Fig. 3(d)).

To demonstrate that f_{rt} is phase-locked to f_{RF}, in Fig. 4 we show four normalized spectra of the injection-locked roundtrip frequency measured with increasing RBW of the SA from 100 kHz to 10 Hz. A −2 dBm RF-power was used in this case, and f_{RF} = 34.69 GHz. By changing the RBW from 100 kHz to 10 Hz, the peak intensity remains constant at 0 dBm whilst the noise floor at a few kHz carrier-offset decreases by 40 dBm. This noise level is determined by the phase-noise of the RF-source. This is confirmed in Fig. 4(d), where the spectrum of the locked f_{rt} is shown together with the spectrum of f_{RF} with a RBW of 10 Hz, the limit of the SA. For the two spectra, the output power of the SA was fixed at −2dBm, and it is clear that the phase noise on both sides of the peak is identical. This confirms that f_{rt} is phase-locked to f_{RF}. To determine the actual phase-noise of the locked f_{rt},, a residual–phase-noise measurement would be needed, but this is beyond the scope of this paper [3,17].

Figure 5 shows the evolution of f_{rt} when increasing the power of the RF-generator, with f_{RF} fixed at 34.706 GHz (Fig. 5(a)), and when increasing f_{RF} to f_{rt}, with the RF power fixed at
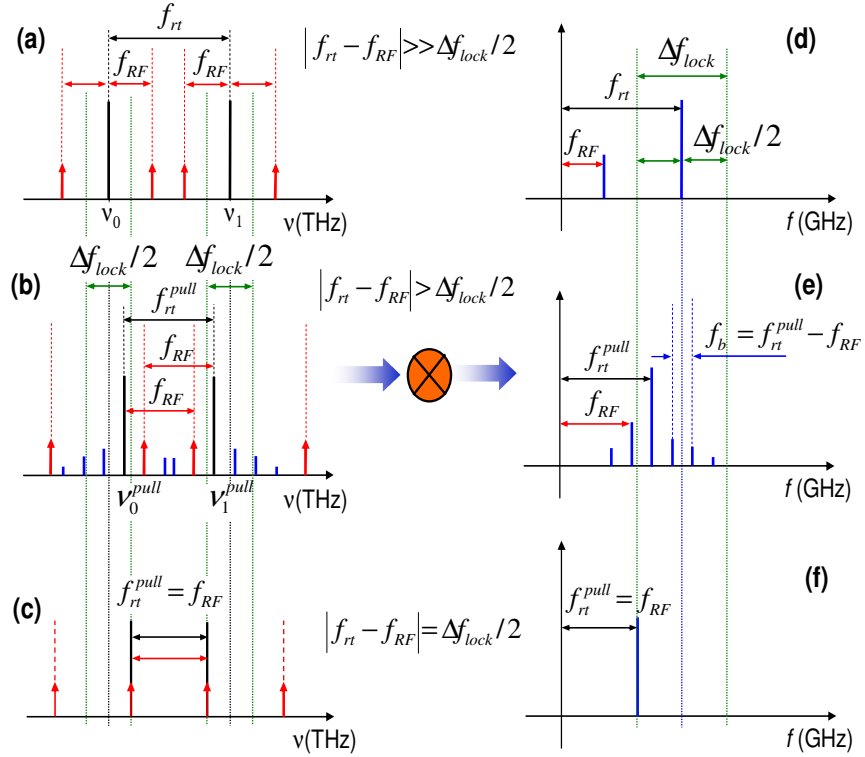
Fig. 7. Schematic diagram showing the RF-injection-locking in the optical ((a), (b) and (c)) and the RF ((d), (e) and (f)), after the rectification process, frequency ranges (see the text for a detailed description).

-2dBm (Fig. 5(b)). In both cases f_{rt} is first pulled and eventually injection-locked to f_{RF}. In particular, when changing f_{RF} for a given RF power (Fig. 5(b)), an interval of RF frequencies can be identified, the so-called *locking-bandwidth* or *locking-range*, where f_{rt} is phase-locked to f_{RF} [22,23]. As an example, Fig. 6 shows a video sample of the SA screen showing the time evolution of f_{rt} when f_{RF} approaches at constant speed from the low frequency side (from left to right), for a fixed RF power of -2 dBm. In agreement with Fig. 4 and 5, initially we observe the pulling of f_{rt} towards f_{RF} and the appearance of multiple sidebands on the right side of f_{rt} [24]. By moving f_{RF} further towards f_{rt}, the latter is eventually injection-locked and remains locked for approximately ~100 MHz. As f_{RF} keeps moving towards higher frequencies, f_{rt} unlocks and sidebands appear on the left side f_{rt} (in agreement with Fig. 5(b)).

The observed injection-locking of f_{rt} is a consequence of the mutual phase-locking of the adjacent longitudinal modes of the laser cavity induced by the AM. Several experimental and theoretical studies of this phenomenon have been carried out using mode-coupled theory since the mid-1960s [22,25,27]. The mechanism of injection-locking in the optical (THz) domain is qualitatively depicted in Figs. 7(a), (b) and (c), of Fig. 7 where for simplicity we have assumed that the free running laser spectrum is composed of two longitudinal modes at frequencies ν_0 and $\nu_1 = \nu_0 + f_{rt}$ (black solid lines). As a result of AM, two RF sidebands are generated on both sides of the FP modes, at $\pm f_{RF}$ (solid red arrows). Well outside the locking range, of width Δf_{lock}, $\mid f_{rt} - f_{RF}\mid \gg \Delta f_{lock}/2$ and the FP modes are running unperturbed (Fig. 7(a)). Closer, but still outside the locking range ($\mid f_{rt} - f_{RF}\mid > \Delta f_{lock}/2$), we observe two phenomena (Fig. 7(b)). First the FP modes start to be pulled by the sidebands, i.e. f_{rt} gets closer to f_{RF}. The pulled f_{rt} is labeled $f_{rt}^{pull} = \nu_1^{pull} - \nu_0^{pull}$, where $\nu_{1,0}^{pull}$ are the frequencies of the pulled FP modes. Secondly, a number of additional sidebands (solid blue lines) are generated

at $v_{1,0}^{pull} \pm nf_b$, where n is an integer and $f_b = f_{RF} - f_{rt}^{pull}$. Inside the locking range $|f_{rt} - f_{RF}| \leq$ $\Delta f_{lock}/2$ and the FP modes are phase-locked by the AM sidebands (Fig. 7(c)). Figure 7(d) to (f) show the RF spectra obtained by the rectification of the optical spectra. As a result of the non-linear conversion process, lines are produced at all possible beating combinations between the optical lines (we note that the locking range in the RF range is twice the locking range in the optical range).
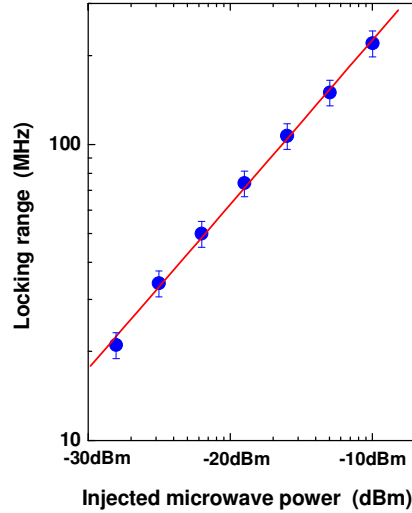
Fig. 8. Metal-metal QCL. Locking range *vs* the RF-power transmitted inside the QCL cavity.

In the case where the frequency of the injected signal is outside the locking bandwidth (Fig. 7(b)), the spectrum of an unlocked oscillator (laser) can be described using Adler's equation [22,27]. In particular the generation of sidebands separated by f_b is predicted as a consequence of a phase-modulation of the pulled laser field by the injecting signal. When the latter is well outside the locking range the modulation is periodic. As the injected frequency gets closer to the limit of the locking range, the intensity of the phase modulation grows, resulting into a stronger distortion of the laser field phase, which gives rise to multiple sidebands. The latter are predicted to be predominantly generated on the opposite side of the pulled oscillator frequency with respect to the frequency of the injected signal [28]. Qualitatively, this description corresponds to what we observe in Fig. 3 and 6, where two sidebands separated by f_b are clearly visible. The fact that we never observe sidebands on the same side of f_{RF} is due to the limited S/N ratio of our measurement (see also the next Section).

In Fig. 8 we show, on a log-log scale, the locking range as a function of the RF-power transmitted into the QCL cavity, i.e. the RF-power from the generator from which the 14dB attenuation is subtracted (see the caption of Fig. 2). Locking ranges up to ~225MHz are observed for 100μW of injected RF-power (i.e. −10dBm inside the device, or ~ + 4dBm from the synthesizer). Considering that the AM frequency is as high as 35GHz, this is an excellent performance, obtained with no specific impedance adaptation. It is mainly the consequence of the following main factors: (i) the relatively low microwave amplitude attenuation provided by the metal-metal waveguide, (ii) the close proximity of 35GHz to the transmission resonance peak of the waveguide, (iii) the rather low operating current of the device, and (iv) the short non-radiative lifetime of the upper laser state [13,14]. All of these factors contribute to reaching high modulation depths. From the measured S-parameters of the device we

compute a small-signal modulation depth of $\sim 9\sqrt{P_{RF}(mW)}$ (mA) at the operating point (see the Appendix for the derivation).
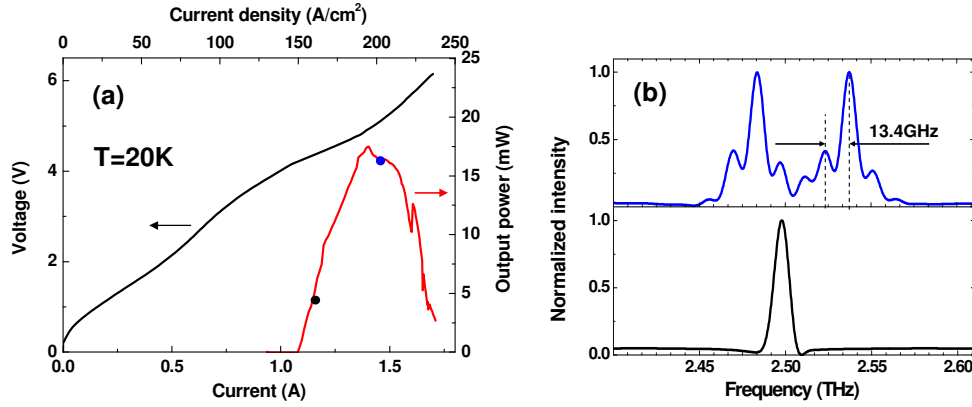
Fig. 9. Single plasmon waveguide QCL. The device is 3mm-long and 240μm wide. **(a)** CW Volage/Current and Optical-power/Current characteristics at a heat-sink temperature of 20K. Note that the emitted power is more than two orders of magnitude higher compared to the metal-metal QCL of Fig. 1 **(b)** Representative THz emission spectra measured at a currents of 1.15A (black dot in panel(a)) and 1.46A (blue dot in panel (a)).

The solid red line in Fig. 8 is the result of a linear fit. The resulting slope is 0.55 ± 0.01, indicating a square-root dependence of the locking-bandwidth on the RF-power. This is in agreement with injection-locking theory, where the relation between the locking-bandwidth and the injected power can be derived for any type of injection-locked oscillator, and is given by [22,27]:

$$\Delta f_{lock} = \frac{2\nu_0}{Q}\sqrt{\frac{P_{inj}}{P_0}}. \tag{1}$$

Here ν_0 is the free-running oscillation frequency, P_{inj} and P_0 are the injected power and the free-running oscillator power respectively, and Q is the oscillator q-factor. Equation (1) is strictly valid for "classical" injection-locking, where one longitudinal mode, of power P_0, of a free-running single or multi-mode laser is injected by a (usually) weak monochromatic source of power P_{inj}. In the case of RF injection-locking the picture is less straightforward. For instance, if more than 2 FP modes are present, except for those at the edge of the spectrum, each FP mode presents two sidebands, one on each side, that in principle compete for injection-locking. We could not find in the literature a rigorous derivation of the locking range in the case of RF-injection-locking. However, from Fig. 7 one can reasonably assume that the ratio P_{inj}/P_0 in Eq. (1) is approximately given by the ratio between the average power of the sidebands and the average power of the FP modes. For a given RF-power injected in the device, this ratio can be derived from the Output Power *vs* Current characteristic presented in Fig. 1, once the current modulation depth is known. Using the value of the modulation depth derived in the Appendix (Eq. (A.2)), from the data of Fig. 8 and Eq. (1), we obtain a cavity q-factor of ~100. We calculate approximately the same value (~110) using an effective modal refractive index of 3.4 and losses of ~16cm^{-1} (including propagation and radiative losses) [29].
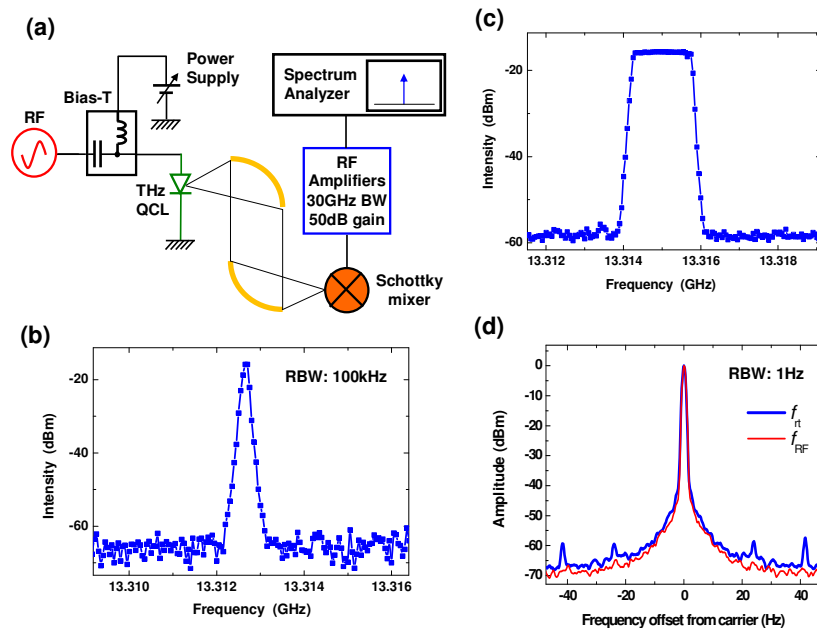
Fig. 10. Single plasmon QCL. (a) Schematic of the measurement setup for the RF injection-locking. The beam from the QCL is coupled on the Schottky mixer using a pair of 90-deg off-axis parabolic mirrors with *f*-numbers of 1 and 2, for collection and focusing respectively. The mixer is a commercial point-contact Schottky diode with an IF-bandwidth of approximately 40GHz, embedded into a corner-cube retro-reflector. The RF-signal from the mixer is first amplified using two wideband amplifier stages of 20 and 30dB gain and finally fed into the SA. (b) Single-shot RF spectrum collected with a RBW of 100kHz and a sweep time of 4ms. The QCL was driven at 1.46A, at a temperature of 20K. (c) Same spectrum of panel (b) collected with the "peak-hold" function of the SA switched ON. The measurement time was of ~10s. (d) Injection-locked spectrum normalized to 0dBm maximum amplitude, and collected with a RBW of 1Hz with 100 video averages (blue line). The RF-power is of 0dBm (for clarity the *x*-axis was offset by the carrier frequency of 13.324GHz). The red line shows the spectrum of the RF-source (Anritsu MG3693B) normalized to 0dB.

3. RF Injection-locking of single-plasmon waveguide THz QCLs

To study injection-locking of a THz QCL with single-plasmon waveguide we used 240-µm-wide waveguide ridges. The active region consists of 90 repeats of the structure presented in Ref [30], which was modified to obtain an emission frequency centered at 2.5THz. The electrical and optical characteristics of a 3mm-long device are displayed in Fig. 9, with the laser driven in CW at a heat-sink temperature of 20K. Two representative spectra are shown in Fig. 9(b) at currents of ~1.15A and 1.46A (black and blue dots in in Fig. 9(a)). Initially the QCL is single mode. At higher currents, multi-mode emission is observed over approximately 10 FP modes, separated by a roundtrip frequency of ~13 GHz. The maximum output power is in excess of 15 mW. This relatively high power, combined with the well-known low beam-divergence of single-plasmon waveguide QCLs (see Ref [31].), allowed the device to be used for pumping a room-temperature THz mixer [20,32]. The latter is a commercial point-contact Schottky diode with an IF-bandwidth of approximately 40GHz, (Farran Technology, Model CM(X)-5) embedded into a corner-cube retro-reflector. As shown in Fig. 10(a), the beam from
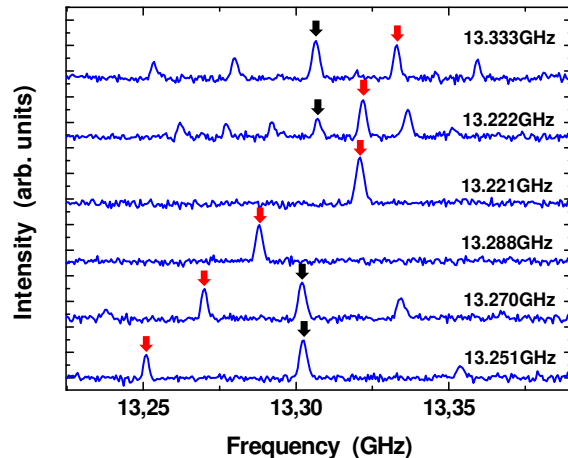
Fig. 11. Single plasmon QCL. RF spectra obtained by sweeping f_{RF} across the locking range, from 13.251GHz (bottom) to 13.333GHz (top). Spectra were collected with + 6dBm of RF-power, a RBW of 100kHz, and a sweep time of 4ms with 5 video averages. The QCL was driven at a current of 1.46A. Similarly to Fig. 4-6, the f_{rt} (black arrows) is pulled towards f_{RF} (red arrows) and a set of sidebands are generated. In the two central spectra f_{rt} is injection locked. The locking range is of approximately 70MHz.

the QCL was coupled to the mixer using a pair of 90° off-axis parabolic mirrors with f-numbers of 1 and 2, for collection and focusing respectively. The RF-signal from the mixer was first amplified using two wideband amplifier stages of 20 and 30dB gain, and finally fed into the SA. To bring the RF signal to the QCL, due to the geometry of the single-plasmon waveguide, it was not possible to exploit the 50Ω-coplanar probe used for the metal-metal device. Therefore the RF signal was brought to the device using 50Ω microstrip-line [15]. The inner conductor of the SMA cable was brought into mechanical contact with one end of the microstrip-line. The other end of the microstrip-line was then wire-bonded to the QCL.

Figure 10 shows different RF spectra of the mixer output with the QCL driven at a current of 1.46 A at T = 20 K. Figure 10(b) presents a single-shot spectrum, with a RBW of 100 kHz and a sweep time of 4 ms. A peak at f_{rt} ~13.3GHz is observed, with a 3dB linewidth of ~100 kHz, limited by the RBW. The spectrum of Fig. 10(c) was obtained instead by switching on the "peak-hold" function of the SA, whilst keeping the same RBW and sweep time. Since the measurement time was approximately 10s, Fig. 10(c) shows a considerable widening of the peak compared to Fig. 10(b), due to a slow random drift of f_{rt} [32,33].

As previously reported [32,34], the set-up shown in Fig. 10(a) leads to a strong feedback on the QCL that we could not avoid. In particular, the position of the RF beat-note can be moved by several MHz by changing the position of the QCL/corner-cube mixer. We cannot quantify the effect of this feedback on the linewidth. However, the fact that the spectral linewidth of Fig. 10(b) is comparable to that found for the THz QCL of Fig. 2 with a metal-metal waveguide, seems to indicate that the external feedback is not dominant. Indeed, for the metal-metal waveguide QCL, there were no optical elements that could couple back the emitted radiation into the device. In addition it is well-known that owing to the strong mode confinement, metal-metal waveguides present very high facet reflectivities, of the order of 90% at 2.4THz, and, more importantly, generate non-directional far-field patterns, with the radiation virtually emitted in all the solid angle [35,36]. All these facts should heavily reduce any feedback coupling.
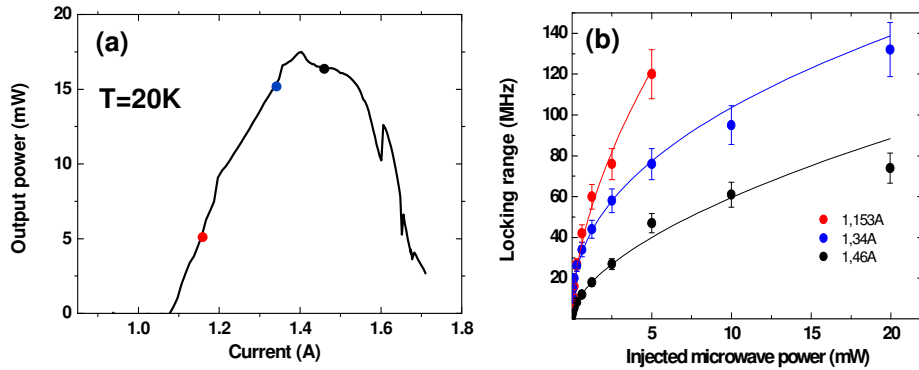
Fig. 12. Single plasmon QCL. (a) Optical-power/ Current characteristic at a heat-sink temperature of 20K. (b) Locking range as a function of RF-power from the synthesizer for different operating currents (red, blue and black dots in panel (a)). The solid curves are the results of fits using $y = a\, x^b$ as fitting function, where y is the locking range, x the injected power, and a, b are fitting parameters. From the lower to the higher current the b-coefficients are 0.57 ± 0.02, 0.42 ± 0.01 and 0.57 ± 0.01, respectively.

As for the metal-metal waveguide device, we used an RF-synthesizer to AM the QCL and injection-lock f_{rt}. As an example of injection-locking, Fig. 10(d) shows (blue line) the locked spectrum normalized to 0dB maximum amplitude, and collected with a RBW of 1Hz, the highest of our SA (for clarity the x-axis was offset by the carrier frequency) [37]. The power of the RF-source was of 0dBm, with a sweep time of 2.3s, and 100 video averages. For comparison we have superimposed the spectrum of the RF-source (Anritsu, MG3693B) normalized to 0dB. Except for a slightly higher phase noise of ~2dB, which at the moment we do not explain, the locked f_{rt} overall presents a phase noise comparable to that of the generator (~-70dBm/Hz at 50Hz offset).

We verified (not shown) that the same results reported in Fig. 10 could be replicated by measuring the RF spectrum of the QCL bias-voltage with the setup of Fig. 2(a), confirming that the "integrated" rectification technique is a valid tool to measure the RF frequency and phase stability of the QCL.

Figure 11 shows a set of spectra obtained by sweeping f_{RF} across the locking range, from low to high frequencies. Similar to Fig. 4–6, f_{rt} (black arrows) is pulled towards f_{RF} (red arrows) and a set of sidebands is generated. In the two central spectra f_{rt} is injection locked. Outside the locking bandwidth we observe the presence of sidebands separated by f_p, which, on the top two traces, appear on both sides of f_{rf}. However, as predicted by Adler's equation, the sidebands appear predominantly on the opposite side of f_{rt} with respect to f_{RF} [28].

Figure 12(b) shows, on a linear scale, the locking ranges as a function of the RF-power at the output of the synthesizer for three different currents (see the dots in Fig. 12(a)). The solid curves are the results of fits using $y = a\, x^b$ as fitting function, where y is the locking range, x the injected power, and a, b are the fitting parameters. From the lower to the higher current, the fits yielded b-coefficients of 0.57 ± 0.02, 0.42 ± 0.01 and 0.57 ± 0.01, showing a good agreement with the value of 0.5 predicted by Eq. (1). The maximum locking ranges obtained are of 119MHz (7dBm RF-power at 1.153A), and 134MHz and 79MHz (13dBm RF-power at 1.34 and 1.46A respectively). We verified (not shown) that the locking ranges are identical regardless of the sign of the detuning of f_{RF} with respect to f_{RT}. From Eq. (1) it appears that for a given power of the RF generator the locking range is proportional to $\sqrt{P_{inj}}$.
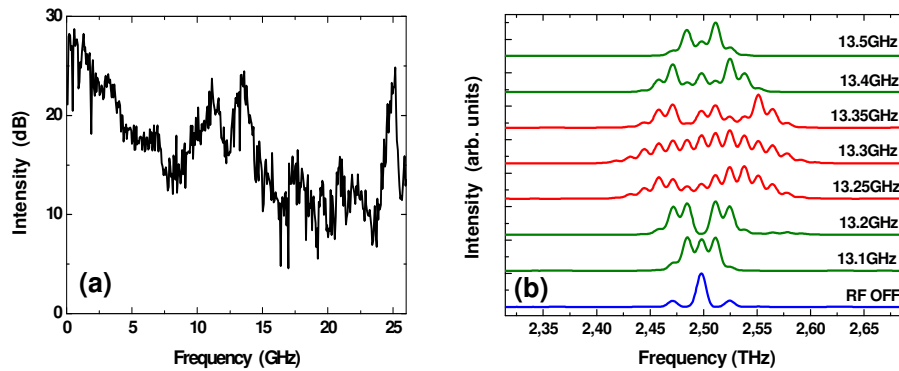
Fig. 13. Single plasmon QCL. (a) Normalized optical-modulation response in the range 100MHz-26GHz. The trace was obtained by sweeping the frequency of the RF-generator at a constant power of 5dBm, and by collecting the signal from the Schottky with the max-hold function of the SA switched ON. The signal from the Shottky mixer was amplified with a 30dB gain, 30GHz bandwidth amplifier. The QCL drive current was of 1.2A. (b) Emission spectra of the QCL at a current of 1.34A, without RF (blue curve), and with an RF-power of 20dBm. The green and red spectra were collected with f_{RF} outside and inside the locking range respectively.

In the small signal approximation, the latter quantity is proportional to the product of the current modulation depth (see the Appendix) multiplied by the square root of the first derivative of the Light-Current characteristic of the device. From Fig. 12(a) it appears that this slope decreases as the current is increased from 1.153A to 1.34 and then 1.46A. This explains qualitatively the reduction of the locking range. For a quantitative comparison one should calculate the current modulation depth, which in turns depends, at each operating current, on the device impedance at f_{rt} (see the Appendix). For the metal-metal waveguide the latter was derived from the measurements of the S-parameters [14]. For the single-plasmon waveguide QCL we did not perform such a characterization, and therefore a derivation of the modulation depth is not possible. We could however measure the small signal optical modulation response function of the QCL + RF-package assembly with the setup of Fig. 10(a), assuming a flat RF-response of the Schottky mixer up to ~30GHz as specified by the manufacturer. For this measurement the IF output from the Schottky diode was amplified using a wideband amplifier with 30dB gain and a 3dB-bandwidth of 30GHz. The QCL was driven at 1.2A. As shown in Fig. 9(b) at this current the device is single-mode, therefore the AM of the QCL produces a single beat-note signal at f_{RF} on the SA, generated by the beating between the carrier frequency and the modulation sidebands (to rule-out possible parasitic RF-couplings we verified that by blocking the THz beam the signal at f_{RF} disappeared).
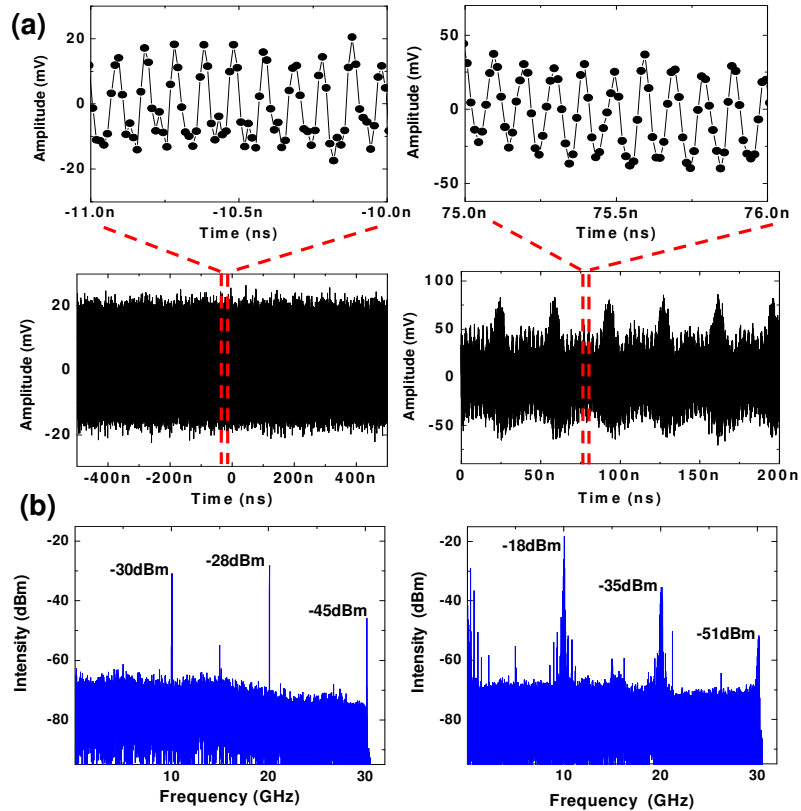
Fig. 14. 4-mm long single plasmon QCL. (a) Single shot traces measured on a time window of 1ns. The top traces are an expanded section of the middle ones on a time window of 1μs. In the left traces the QCL is injection-locked at f_{RF} = 10.042GHz and with an RF-power of + 6dBm. In the right traces f_{RF} = 10.098GHz, i.e. at the edge of the locking range. The RF-power is of + 14dBm. (b) Fourier transforms of the corresponding (left and right) top traces of panel (a). The intensities of the fundamental 2nd and 3d harmonics of f_{rt} are reported next to each line. In the right panel a number of sidebands can be seen around each harmonic.

Figure 13(a) reports the normalized optical-modulation response of the QCL in the range 100MHz-26GHz. The trace was obtained first by sweeping the frequency of the RF-generator at a constant power of 5dBm, and by collecting the signal from the Schottky mixer with the max-hold function of the SA switched ON. Next the curve was normalized to the transmission of the SMA cables and bias-T (Fig. 10(a)). We observe an initial drop up to 8GHz with a slope of ~-15dB/decade. Then the modulation response grows and two peaks of ~-5dB attenuation appear at frequencies of ~11.0 and 13.5GHz, i.e. close to f_{rt} (Fig. 10). These are the result of unintentional partial impedance matchings. Beyond 15GHz the response remains flat at ~-17dB attenuation. Another peak is observed at ~25GHz, which we attribute to another partial impedance matching.

Figure 13(b) shows the effect of the AM on the emission spectrum of the QCL when f_{RF} is in proximity to f_{rt}. In this case (see also Fig. 7) the RF sidebands are amplified by the laser regenerative gain close to the FP modes [22]. Besides the pulling and locking effects already described, this contributes to bring more FP modes above threshold. As shown in Fig. 13(b) for a current of 1.34A, with the RF-generator OFF the spectrum is composed of 3 longitudinal modes separated by twice f_{rt} (blue line). Switching ON the synthesizer with an RF-power of 20dBm strongly affects the spectrum. Outside the locking range (green lines) the RF modulation brings missing longitudinal modes above threshold. Inside the locking range (red

lines) the number of FP modes increases abruptly, with up to 14 longitudinal modes above threshold at 13.3GHz, yielding a spectral bandwidth of ~190GHz. The fact that inside the locking range the FP modes are mutually phase-locked (Fig. 7) means that the QCL is operating in a regime of active mode-locking, emitting a train of pulses with a timing jitter determined by the phase noise of the RF-generator. At the moment the lack of suitable techniques prevents the measurement of the pulse length and shape. We have, however, exploited the elevated IF bandwidth of the Schottky mixer to acquire single shot traces using a fast oscilloscope (LeCroy WaveMaster 870Zi) with a real time bandwidth of 30GHz (20ps rise time). Although this bandwidth is too limited to reveal the pulse duration, it has anyway allowed us to show the distortion produced on the THz waveform when the RF signal is brought just outside the locking range. In fact the *ac* signal at the output of the mixer results from the beating of the optical sidebands around each FP mode (see Fig. 7). As such it represents the temporal envelope of the THz wave emitted by the QCL. Inside the locking range, i.e. in mode-locking operation, the temporal shape of the lasers consists of a series of identical pulses arising from all equally spaced longitudinal modes phase-locked by the AM. Out of the locking range the system has a very different temporal behavior as now the longitudinal modes beating interferes with f_{RF}.

For these measurements we used a ~4mm-long single-plasmon ridge, yielding f_{rt} ~10GHz. This allowed us to have the 3rd harmonic of f_{rt} at the edge of the measuring system bandwidth (see below) [38]. The output signal from the Schottky mixer was amplified using a 30GHz-bandwidth amplifier with a gain of 26dB. The QCL was driven at a current of 2.036A. At this current we measured a THz spectrum (not shown), composed approximately 10 FP modes separated by f_{rt} ~10GHz. Figure 14 displays two representative single shot traces measured on a time window of 1μs, corresponding to approximately 10^4 round trips (Fig. 14(a)). The corresponding Fourier transforms are shown in Fig. 14(b). In the left traces of panels (a) and (b) the QCL is injection locked at f_{RF} = 10.042GHz with an RF-power of + 6dBm. In the Fourier transform (panel (b)), the fundamental, the 2nd, and the 3rd harmonic of f_{rt} are clearly visible, with intensities of −30dBm, −28dBm, and −45dBm respectively (we note that the 3rd harmonic is at the edge of the system bandwidth and therefore suffers from an additional ~10dB attenuation compared to the other lines). The fact that no other peaks are present between the harmonics indicates negligible distortion of the emitted pulse train within the probed bandwidth of 30GHz (the line at ~15GHz is not due to the THz field) [5]. This is confirmed by the time trace of Fig. 14(a) showing a stable amplitude. The expanded view shows the same trace on a time window of 1ns. The pulses show a bandwidth limited duration of ~35ps. From the THz spectra, and assuming that the FP modes have an equal phase, the expected pulse duration is of ~10ps.

In the right traces of Fig. 14(a) and Fig. 14(b), f_{RF} = 10.098GHz, i.e. just outside the locking range (the RF-power is of + 14dBm). As shown in the bottom spectrum this generates a large amount of sidebands around each harmonic of the roundtrip frequency. By zooming on the harmonics we find (not visible in the spectrum of Fig. 14) that the lines are separated by f_b = 29MHz, and we also observe a number of intense lines separated by ~377MHz = 13 x f_b. Contrary to the left trace of panel (a), the resulting time trace is strongly distorted, with a slow modulation at f_b = 29MHz (1/34.5ns) superimposed to a fast component at 377MHz (1/2.65ns). The expanded section shows the time trace in a window of 1ns. Compared to the expanded section of Fig. 14(a) the shape is closer to that of a sinusoid with a period of 100ps, and a measured "pulsewidth" of ~50ps . This is in agreement with the fact that the intensity of the fundamental is of −18dBm compared to only −35dBm and −51dBm for the 2nd and 3rd harmonics respectively.

4. Conclusions

In this work we have demonstrated that RF injection-locking using AM is a valid technique that allows phase-locking of the roundtrip frequency of THz QCLs to an RF synthesizer. Using devices based on metal-metal as well as single-plasmon waveguides, we have taken advantage of the high modulation bandwidths of THz QCLs, of several tens of GHz and more [14], to show that locking ranges up to a few hundreds of MHz can be achieved with modest RF-power levels. Inside the locking range the phase noise of the roundtrip frequency is equal to that of the RF-synthesizer, showing a linewidth of 1Hz, that is limited by the resolution bandwidth of our SA. This means that under roundtrip injection the longitudinal FP modes are mutually phase-locked, i.e. the QCL is mode-locking and emitting a pulse train with a pulse to pulse timing jitter determined by the RF-generator. In this context we recall that mode-locked operation of QCLs has been a very controversial subject, with the first claims of passive and active mode-locking of QCLs operating in the MIR range [9,39] subsequently re-interpreted as coherent dynamic instabilities resulting from the extremely fast gain recovery time, of ~1ps, of this family of lasers [40,41]. Only recently, mode-locking of a QCL operating at 6.3μm has been demonstrated using an *ad hoc* active region, where the non-radiative upper state lifetime (and thus the gain recovery time) was artificially raised to several tens of ps [9]. Compared to mid-IR QCLs it is well known that THz QCLs, in particular those based on bound-to-continuum active regions like the one used in this work, present significantly larger non-radiative relaxation times of the upper laser state, of ~5-10ps, owing to the fact that the laser transition energy lies below the optical phonon [42–44]. We speculate that this fact could be determinant for the results found in this work.

5. Appendix

To calculate the small signal current modulation depth of the metal-metal device we recall that the value of the RF-power dissipated in the QCL is given by [45]:

$$P_{diss} = \frac{\delta I_{qcl}^2 \cdot \mathrm{Re}[Z_{qcl}]}{2}, \qquad (A.1)$$

where δI_{qcl} is the peak current variation around the operating point induced by the RF modulation and Z_{qcl} is the complex impedance of the device at f_{RF}. The latter can be derived by the measurement of the *S*-parameters of the device. From Ref [14]. we obtain $\mathrm{Re}[Z_{qcl}] \cong 20\Omega$ at 34.7GHz. P_{diss} is equal to the RF-power incident on the device from the 50Ω coplanar probe, P_{RF}, multiplied by the transmission coefficient. The latter can be obtained from the $1-|S_{11}|^2$ curves reported in Ref [14]. At 34.7GHz we measure a transmission coefficient of 0.8 (~1dB). From Eq. (A.1) we therefore obtain:

$$\delta I_{qcl}(mA) = 9\sqrt{P_{RF}(mW)}, \qquad (A.2)$$